

Where are the earliest stars relics in the simulated Milky Way analogues?

HANG YANG ^{1,2,3} LIANG GAO ^{1,4,2} QI GUO ^{2,3,4} HAINING LI ² SHI SHAO ² AND GANG ZHAO ^{2,3}

¹*School of Physics and Laboratory of Zhongyuan Light, Zhengzhou university*

²*National Astronomical Observatories, Chinese Academy of Sciences, Beijing 100101, China*

³*School of Astronomy and Space Science, University of Chinese Academy of Sciences, Beijing 100049, China*

⁴*Institute for Frontiers in Astronomy and Astrophysics, Beijing Normal University, Beijing 102206, China*

ABSTRACT

Using 6 Milky Way analogues with two different numerical resolutions from the Auriga simulation, we investigate the total mass, spatial distribution and kinematics of the earliest stars relics in the Milky Way at $z = 0$. These relics (second generation stars) formed over a wide redshift range, from about $z = 22$ to $z = 4$, with an average formation redshift of $z \sim 10.0$, and comprise about 2×10^{-5} of the entire galactic stellar population. The disk and bulge components host only a small fraction of these relics, contributing less than 12 percent in total. The stellar halo, in particular the outer stellar halo of which galactic radius $r > 30$ kpc, hosts the largest fraction (about 46 percent on average), with an average of one relic star for per 4,000 to 10,000 stars, making it a promising region for observational searches. Additionally, around 18 percent of the earliest stars relics are found in satellite galaxies, with smaller and older satellite galaxies tending to contain a higher proportion of these stars. Thus, low-mass and early-formed satellite galaxies are also ideal targets for finding such relics, although some satellite galaxies may lack them entirely. The spatial distribution and kinematics of these stars show good numerical convergence across different simulation resolutions. Our results provide valuable guidance for searches of the earliest stars relics and offer insights for interpreting findings from ongoing and future stellar archaeology surveys.

Keywords: Milky Way Galaxy (1054); Galactic archaeology (2178); Population II stars (1284); Hydrodynamical simulations (767)

1. INTRODUCTION

The first generation stars (also often referred to as population III stars, or Pop III stars) are thought to have been born from primordial gas (e.g. [Abel et al. 2002](#); [Yoshida et al. 2003, 2006](#); [Reed et al. 2005](#); [Gao et al. 2007](#)) in the early Universe about few hundreds Myrs after the Big Bang. In the standard Λ CDM paradigm, primordial gas could condense in dark matter halos with a virial mass about $10^6 M_{\odot}$ molecular cooling (e.g. [Tegmark et al. 1997](#)), and then form the first stars once their density became sufficiently high. The formation of the Pop III stars end the dark ages of the Universe, prompt chemical enrichment and initiating the reionization of the Universe. Although such classical formation scenarios have been proposed ([Bromm &](#)

[Larson 2004](#); [Bromm & Yoshida 2011](#); [Klessen & Glover 2023](#), for an overview), properties of the Pop III stars remain uncertain. For example, their initial mass function (IMF) is still highly uncertain.

Although the statistical properties of the first generation stars are shaped by many complex and competing physical processes (such as fragmentation, mergers, radiation feedback, etc.), it is generally believed that the Pop III stars have a top-heavy IMF (e.g. [Stacy et al. 2016](#); [Hirano & Bromm 2017](#)). In this scenario, most Pop III stars evolve rapidly and soon end their lives either as supernovae (SNe) explosion or by collapsing into black holes directly, depending on their mass (e.g. [Schaerer 2002](#)). The SNe of Pop III stars would eject metals into the surrounding environment, enriching the gas and enabling it to re-collapse, thereby forming the second-generation stars. These bona fide second-generation stars are usually expected to be high carbon-enhanced, and possible carry the unique elemental abun-

dance patterns (e.g., the strong odd–even effect for pair-instability supernovae (PISNe) descendants) that could trace the properties of their progenitor Pop III stars (e.g. Heger & Woosley 2002; Aoki et al. 2014; Ji et al. 2015). One of the most feasible methods to constraint the properties of first generation stars is through stellar archaeology surveys in our Galaxy (e.g. Hartwig et al. 2015; Ishigaki et al. 2018; Li et al. 2022). By comparing the theoretical nucleosynthetic yields of Pop III SNe with the chemical composition of surviving second-generation stars in the nearby Universe, it becomes possible to infer the properties of Pop III stars. For instance, Xing et al. (2023) identified the chemical signature of PISNe in a metal-poor star in the Milky Way, indicating a super massive Pop III star progenitor with an initial mass approximately of $260 M_{\odot}$. Such observations provide direct constraints on the properties of Pop III stars. In addition, some theories predict the long-living low mass ($M_* < 0.8M_{\odot}$) Pop III star (e.g. Greif et al. 2011; Susa et al. 2014; Ishiyama et al. 2016; Magg et al. 2018). The discovery of such stars will directly constrain the lower mass limit of the Pop III IMF. Since the number of these earliest stars relics (hereafter referred to as ESR) in the Milky Way is expected to be very rare, the total mass, spatial distribution and kinematics of these ESR are critical information for stellar archaeology study.

In the past decade, studies based on both semi-analytic methods (e.g. Scannapieco et al. 2006; Gao et al. 2010) and cosmological hydrodynamical simulations (e.g. Starkeburg et al. 2017; El-Badry et al. 2018; Sestito et al. 2021; Chen et al. 2023; Sotillo-Ramos et al. 2023) have aimed to predict the distribution of the ESR in the Milky Way. Most of the cosmological hydrodynamical simulations, however, do not explicitly model the Pop III stars formation. Hence, the bona fide second-generation stars cannot be included in these simulations. Instead, they often adopt extremely metal poor stars (EMP stars; $[\text{Fe}/\text{H}] < -3$) as the proxies for ESR. In these simulations, the enrichment of EMP stars origin from the stars formed in the atomic cooling halos (first galaxy halos) rather than the genuine Pop III stars, which were born in molecular cooling halos. In real world, accounting for enrichment from these stars would wipe out the Pop III abundance signatures in EMP stars and weaken the constraints on properties of Pop III stars (e.g. Ji et al. 2015). Moreover, some studies have shown that the metallicity of ESR is not necessarily lower than $[\text{Fe}/\text{H}] = -3$ (e.g. de Bannassuti et al. 2017; Magg et al. 2022; Xing et al. 2023).

In this short paper, we make use of the Auriga simulation and adopt a more reasonable tracer for the ESR, to explore their spatial distribution and kinematics at

present day. Our results might provide valuable guidance for hunting ESR and interpreting results from ongoing and future surveys. The structure of this paper is as follows: in Section 2, we describe the numerical simulation and methodology. The main results are presented in Section 3, and we conclude with a summary of our findings in Section 4.

2. METHOD

2.1. Cosmological simulation

The Auriga project (Grand et al. 2017) comprises a suite of zoom-in cosmological simulations of Milky Way-mass dark matter halos and their surroundings. The parent Auriga halos were selected from a dark matter only simulation of the EAGLE (Schaye et al. 2015) project. The Auriga projects were performed with the magneto-hydrodynamic moving mesh code AREPO (Springel 2010), and the adopted cosmological parameters are $\Omega_m = 0.307$, $\Omega_b = 0.048$, $\Omega_{\Lambda} = 0.693$, $h = 0.6777$, $n_s = 0.9611$ and $\sigma_8 = 0.829$ (Planck Collaboration et al. 2014). The basic information of the Milky Way analogues are shown in Table 1. The main implements of galaxy formation in Auriga include primordial and metal line cooling; a spatial uniform UV background that completed HI reionization at $z = 6$; a two phase ISM model; a stochastic star formation model in cell with gas number density larger than $n = 0.13 \text{ cm}^{-3}$; stellar and AGN feedback. A more detailed description of the Auriga model can be found in Grand et al. (2017).

Two different resolution runs, level-3 and level-4, are used in this paper, which correspond to the dark matter (baryonic) mass resolution of about $5 \times 10^4 M_{\odot}$ ($6 \times 10^3 M_{\odot}$) and $4 \times 10^5 M_{\odot}$ ($5 \times 10^4 M_{\odot}$), respectively. For brevity, we use L3 and L4 to refer to these two resolution runs in the following sections. The Friends-of-Friends (Davis et al. 1985) and SUBFIND (Springel et al. 2001) algorithms were applied to construct halo and subhalo catalog.

2.2. Earliest stars relics sample

Due to the limitations of the numerical resolution and sub-grid physics models, most cosmological simulations are unable to resolve the first generation stars formation, including the Auriga project used in this work. Previous numerical studies have shown that the central region of first galaxies have already been enriched by early Pop III stars (e.g. Greif et al. 2010; Wise et al. 2012), hence the very first stars formed in the first galaxies contain most direct information on properties of Pop III stars. While the gas physics in the first galaxy formation is not realistic in the Auriga simulation suites because the gas of such systems is in the un-enriched primordial state,

Table 1. The general properties of the simulated central galaxy at $z = 0$. From left to right, the columns are: (1) simulation name; (2) virial radius for host halo; (3) virial mass for host halo; (4) total stellar mass for central galaxy.

Name	R_{200} [kpc]	$\log_{10} M_{200}$ [M_{\odot}]	$\log_{10} M_{*}$ [M_{\odot}]
Au6-L4	213.8	12.02	10.72
Au6-L3	211.8	12.0	10.81
Au16-L4	241.5	12.18	10.83
Au16-L3	241.5	12.18	10.96
Au21-L4	238.6	12.16	10.91
Au21-L3	236.7	12.15	10.94
Au23-L4	245.3	12.20	10.98
Au23-L3	241.5	12.18	10.95
Au24-L4	240.9	12.17	10.87
Au24-L3	239.6	12.17	10.94
Au27-L4	253.8	12.24	11.0
Au27-L3	251.4	12.23	11.0

the closest tracer of the earliest stars relics may be the metal free stars with $[\text{Fe}/\text{H}] = 0$ in the simulations as they are not polluted by any other star formation process in the first galaxies. Therefore, we select the metal free star particles as the earliest stars relics tracers in the Auriga simulation suites. For convenience and to avoid ambiguity, we refer to the earliest stars relics as ESR in the following sections.

2.3. Orbital decomposition

The kinematic features of such ESR sample provide important information for identifying them in observations. We adopt the total angular momentum direction of all stars within 10 kpc as the z-axis and then transform the position and velocity vectors of all star particles into the new galactic center coordinate system. Based on the galactic radius r and circularity, defined as $\epsilon = j_z/rV_c(r)$, the orbit types of such ESR can be separated into four components, 1) the disc stars with $r < 30$ kpc and $\epsilon > 0.7$; 2) the bulge stars $r < 3$ kpc and $\epsilon < 0.7$; 3) halo stars which include the inner halo stars with $r < 30$ kpc and $\epsilon < 0.7$; and 4) the outer halo stars with $r > 30$ kpc. The similar decomposition method have been adopted in previous works (e.g. [Zhu et al. 2022](#); [Chen et al. 2023](#)).

3. RESULTS

3.1. The formation time and total mass of ESR in the Milky Way analogues

It is interesting to see when and how many ESR have been formed in the Auriga simulations. In Fig. 1, we plot the total mass of such stars which end up in virial radius of 6 Auriga halos at $z = 0$ as a function of redshift.

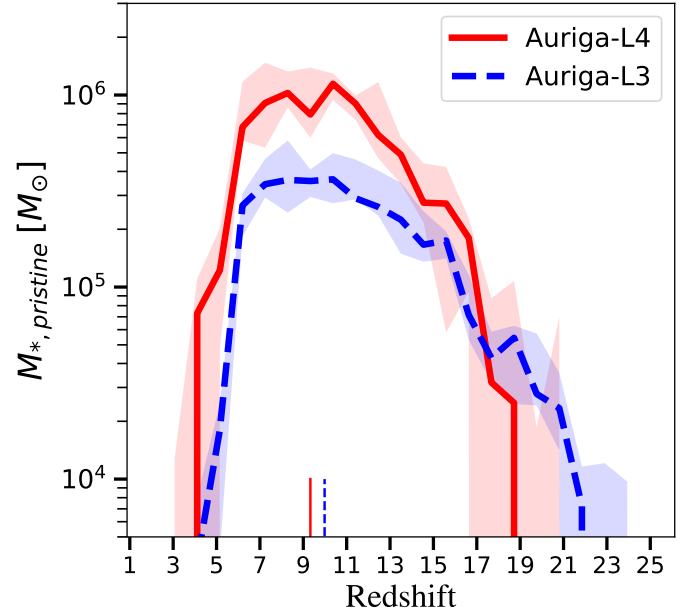


Figure 1. The total mass of formed ESR as a function of formation redshift for six Milky Way analogues in the Auriga simulation suites. Results are presented for two different numerical resolutions. The red (blue) lines represent the median values of all six samples, while the shaded regions indicate the 16th–84th percentiles. The vertical lines represent the half-mass formation redshift of the ESR.

The median values are shown and the shaded regions indicate 16th–84th percentiles, different colors represent different resolution runs. Clearly, the formation time of the ESR span a wide redshift range, from $z \approx 22$ to $z \approx 4$. The average half-mass formation redshift for all ESR is about $z = 10.0$ for the Auriga-L3 and $z = 9.3$ for the Auriga-L4, as indicated by the vertical lines in the Fig 1. Moreover, more than 85 (80) percent ESR have formed before $z = 6$ for Auriga-L3 (L4). Intriguingly, some ESR could form as low as redshift about $z \approx 4$ in the simulations.

In total, the median mass of the ESR in six Auriga simulations at present day is $10^{6.2}$ ($10^{6.6}$) M_{\odot} for the Auriga-L3 (L4), comprise about 2 (5) $\times 10^{-5}$ of the entire galactic stellar population, making them extremely difficult to detect. Note that while the overall trends are similar between the L3 and L4 runs, the divergence in the quantitative results is expected between two different resolution runs because of numerical resolution effect and the constructed star formation model.

3.2. The spatial distribution and kinematic of ESR in the Milky Way analogues

In order to have a visual impression of present day spatial distribution of the ESR, In Fig. 2, we overlay their positions on the underlying dark matter fields in

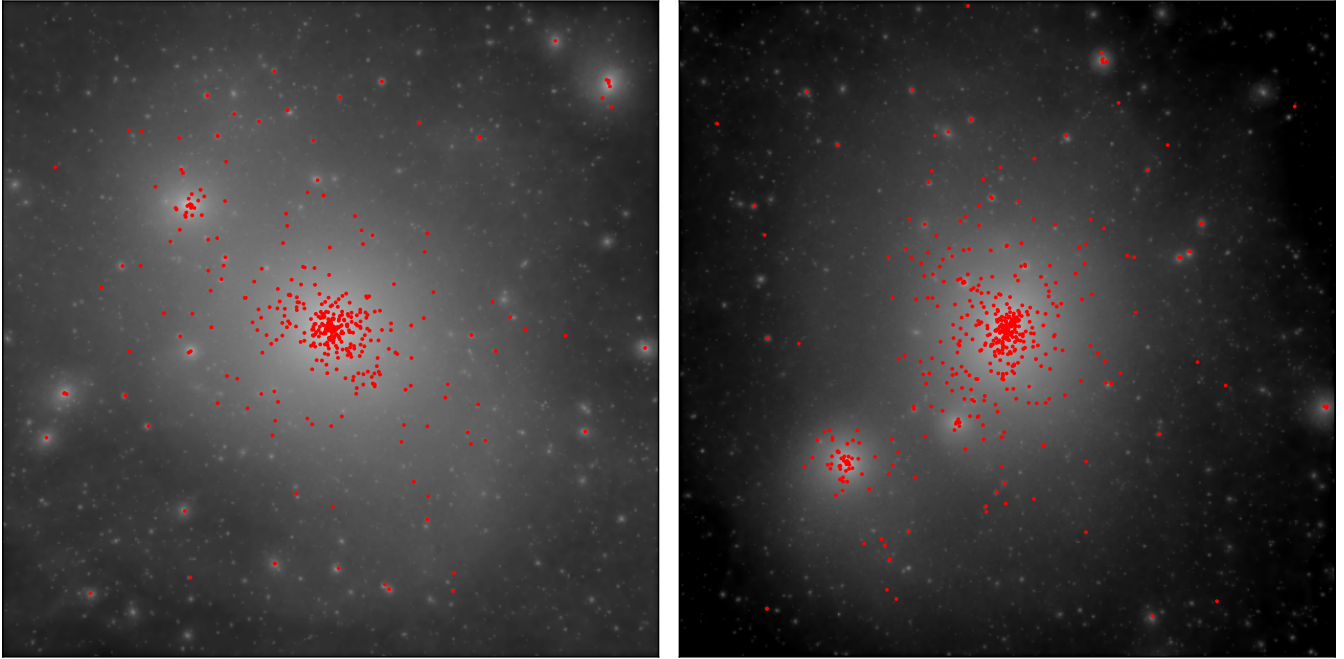


Figure 2. The projected distribution of ESR (red dots) over underlying dark matter density fields of the Au6 (left) and Au16 (right) halos. The results are shown for the level 3 resolution runs. Each panel spans a physical scale of 300 kpc per side.

the Au6-L3 and Au16-L3 runs. The ESR appear concentrated in the central regions of the halos, while a significant fraction is sparsely distributed throughout the stellar halo, and some reside in satellite galaxies. This distribution is a natural consequence of hierarchical structure assembly in cold dark matter theory and is also consistent with the previous studies. The early-formed, low-mass first galaxies gave birth to these ESR. A significant fraction of these first galaxies were disrupted, contributing to the bulge and stellar halo, while some survived as present-day satellite galaxies, still containing their ESR.

In Fig. 3, we show quantitative results for the radial spatial distribution of the ESR in the simulated Milky Way analogues. The bold solid blue and red lines represent the median radial cumulative distributions for Auriga-L3 and L4, respectively. For comparison, we also plot the median radial distribution of all stars in the Auriga simulation suites in bold dashed lines. Clearly, the ESR are substantially less concentrated than the overall stellar population: about half of these stars are located more than 40 kpc away from the galactic center, in stark contrast to the total galactic stellar population, where half of all stars are distributed within 10 kpc of the galactic center. While small differences between different resolution runs are evident in relatively inner regions, the overall numerical convergence is good.

We present the kinematically decomposed results for all stars and the ESR in six Milky Way analogues from

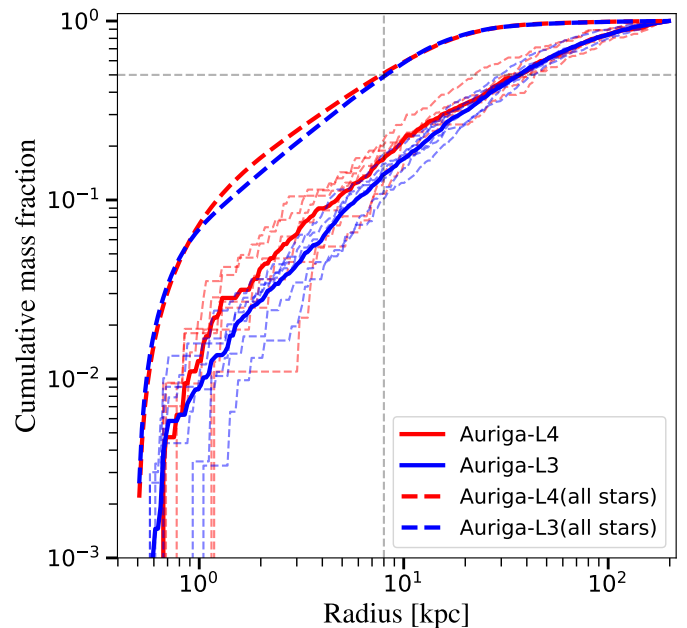


Figure 3. The radial distribution of the ESR and all stars in Milky Way analogues at $z=0$. The bold solid lines represent the average radial distribution of the ESR, while the dashed lines indicate the average distribution of all stars, as specified in the legend. The light-colored lines correspond to results from individual simulated samples.

L3 and L4 simulations in Fig.4 and Fig.5, respectively. Note that we exclude stars associated with satellite galaxies, which account for a significant fraction of the

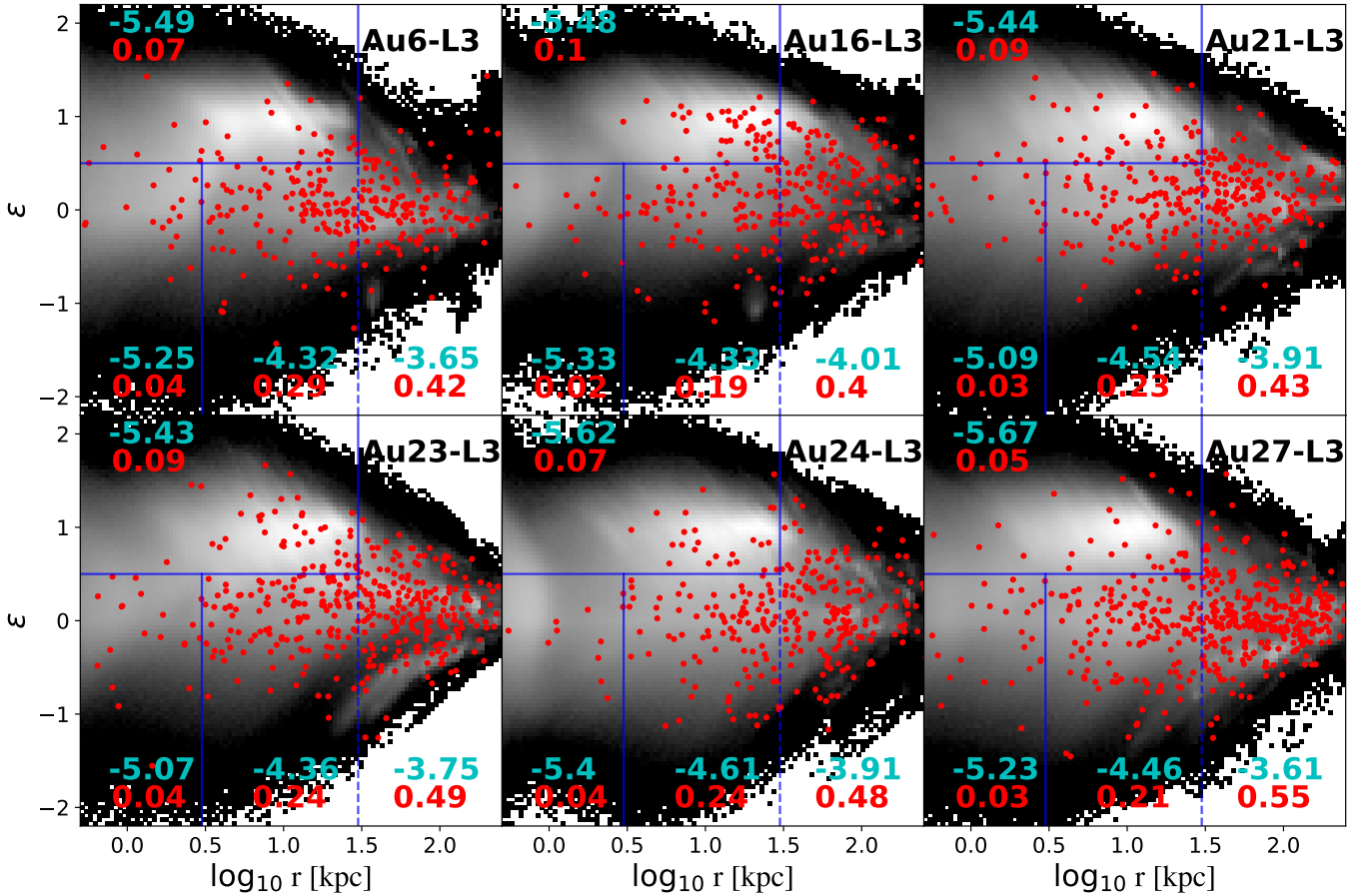


Figure 4. The grey 2D histograms depict the orbital distribution of all stars in the central galaxy of the Auriga-L3, while the red dots represent the orbital properties of individual ESR. The regions outlined by blue lines correspond to different orbital types. The cyan numbers in each region indicate the mass ratio (logarithmic to base 10) of ESR with the corresponding orbital type to all stars, while the red numbers show the mass ratio of ESR with the corresponding orbital type to the total ESR population.

ESR. As shown in Table 2, this fraction varies from halo to halo, ranging from about 10 percent to 30 percent. Comparing the stellar orbit distribution $p(r, \epsilon)$ of all stars, the red dots represent the orbital features for individual ESR in Fig.4 and Fig.5. The red and cyan numbers in each panel show the ratio of ESR of the corresponding orbit type to all ESR and to all stars with the same orbit type, respectively. Note that the cyan numbers are expressed in logarithmic base 10. For reference, these numbers are also listed in Table 2.

As shown in Fig.4 and Fig.5, the stellar halo hosts the largest fraction of ESR, particularly the outer stellar halo, which contains about 46 (49) percent of them in Auriga-L3 (L4), respectively. The fraction of ESR in the bulge is the lowest, at only a few percent, at about 4 (5) percent in Auriga-L3 (L4). Taking into account the strong dust extinction and also high stellar density in the bulge, it is quite challenging to search for these stars observationally in this region. Consistent with expectation

that ex-situ stars are generally believed to have pressure-supported orbits, the proportion of ESR in the disk is also quite low, at about 8 percent. These results suggest that the stellar halo is the most promising region to observe such stars in our Galaxy, especially in the outer stellar halo. According to the cyan numbers shown in Fig. 4, there should be one ESR star out of every 4,000 to 10,000 stars in the outer halo component of Milky Way analogues in Auriga-L3. In comparison, there should be only one ESR star out of every approximately 100,000 disk stars.

As shown by the red numbers, the orbital distributions are roughly numerically converged in both resolutions. However, compared to the lower resolution runs, the ratio of ESR to all stars is slightly lower in the higher resolution runs, as indicated by the cyan numbers. This difference is due to the higher resolution simulations resulting in both a slightly larger total stellar mass and a smaller ESR mass.

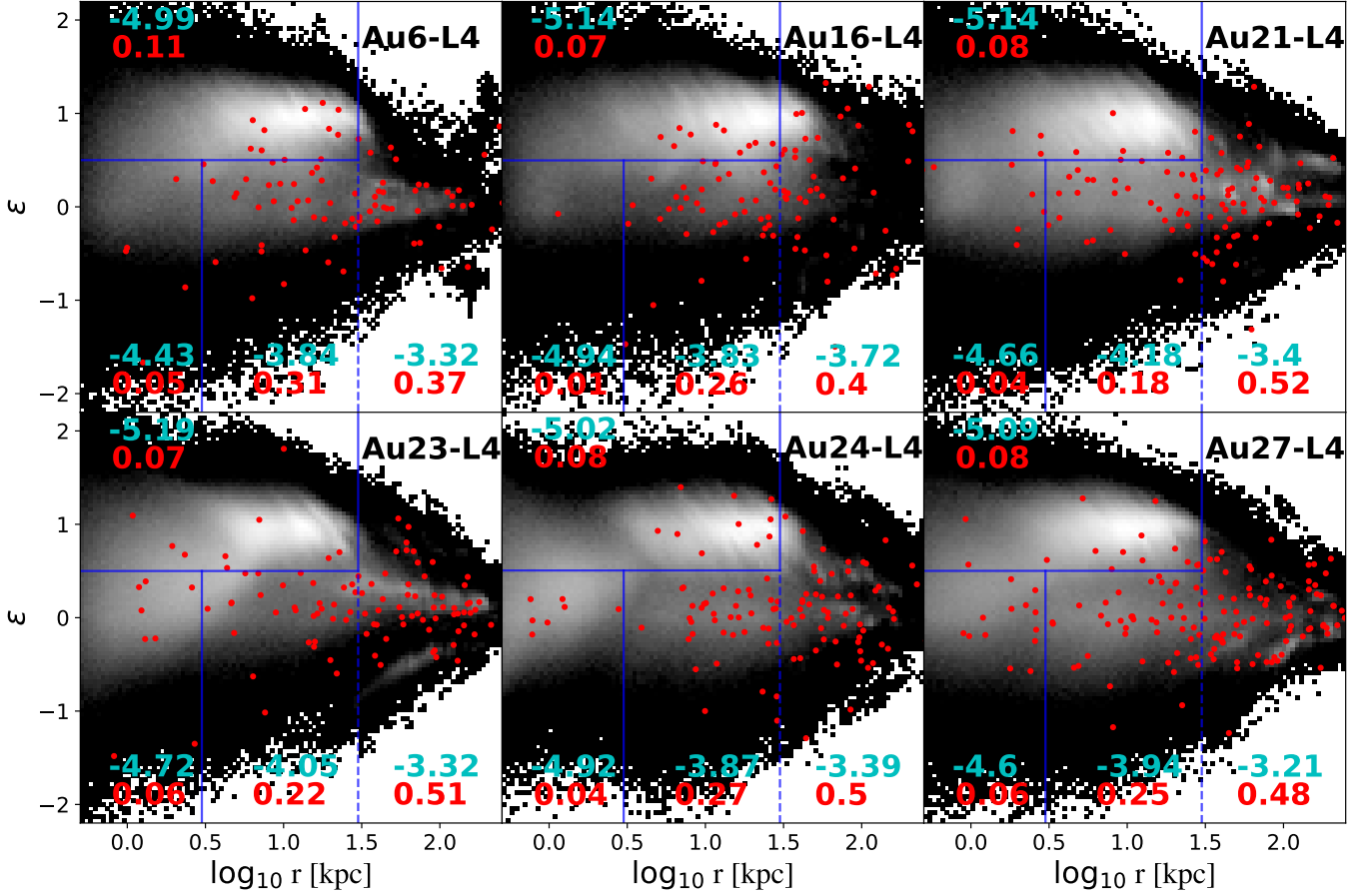


Figure 5. Same as the content of Fig 4, but it is the results for Auriga-L4.

Table 2. The kinematic decomposition of the ESR in each simulated central galaxy at $z = 0$. From left to right, the columns are: 1) ESR in bulge to total relic mass ratio F_B ; 2) ESR in disk to total ESR mass ratio F_D ; 3) ESR in inner halo to total ESR mass ratio F_{iH} ; 4) ESR in outer halo to total ESR mass ratio F_{oH} ; 5) ESR in satellite galaxies to total ESR mass ratio F_S ; 6) ESR in bulge to all bulge stars mass ratio f_B ; 7) ESR in disk to all disk stars mass ratio f_D ; 8) ESR in inner halo to all inner halo stars mass ratio f_{iH} ; 9) ESR in outer halo to all outer halo stars mass ratio f_{oH} .

Name	F_B	F_D	F_{iH}	F_{oH}	F_S	$\log_{10} f_B$	$\log_{10} f_D$	$\log_{10} f_{iH}$	$\log_{10} f_{oH}$
Au6-L3	0.04	0.07	0.29	0.42	0.18	-5.25	-5.49	-4.32	-3.65
Au6-L4	0.05	0.11	0.31	0.37	0.16	-4.43	-4.99	-3.84	-3.32
Au16-L3	0.02	0.10	0.19	0.40	0.29	-5.33	-5.48	-4.33	-4.01
Au16-L4	0.01	0.07	0.26	0.40	0.23	-4.94	-5.14	-3.83	-3.72
Au21-L3	0.03	0.09	0.23	0.43	0.22	-5.09	-5.44	-4.54	-3.91
Au21-L4	0.04	0.08	0.18	0.52	0.18	-4.66	-5.14	-4.18	-3.40
Au23-L3	0.04	0.09	0.24	0.49	0.14	-5.0	-5.4	-4.29	-3.75
Au23-L4	0.06	0.07	0.22	0.51	0.14	-4.72	-5.19	-4.05	-3.32
Au24-L3	0.04	0.07	0.24	0.48	0.17	-5.4	-5.62	-4.61	-3.91
Au24-L4	0.04	0.08	0.27	0.5	0.11	-4.92	-5.02	-3.87	-3.39
Au27-L3	0.03	0.05	0.21	0.55	0.16	-5.23	-5.67	-4.46	-3.61
Au27-L4	0.06	0.08	0.25	0.48	0.13	-4.60	-5.08	-3.94	-3.21

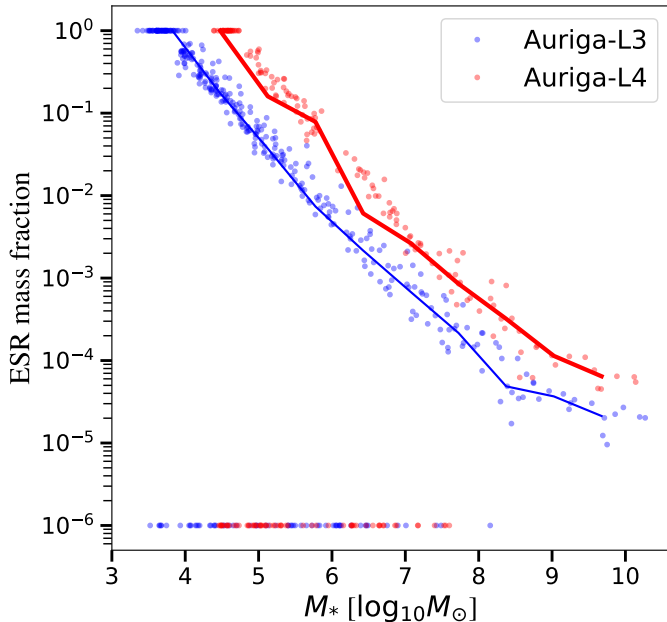


Figure 6. The mass fraction of ESR relative to the total stellar mass (M_*) as a function of stellar mass for each surviving satellite galaxies in all six simulated Milky Way analogues at $z = 0$. For satellite galaxies without ESR, their ESR mass fraction is arbitrarily set to 10^{-6} .

3.3. The ESR in the satellite galaxies

Previous studies suggest that the survival satellite galaxies are also promising sites to hunt for the ESR (e.g. Ji et al. 2015; Jeon et al. 2017). As shown in the Table 2, about 18 percent of the ESR mass budget is in satellite galaxies in Auriga-L3. To identify the best sites to search for the ESR, in Fig. 6, we plot the stellar mass M_* of each simulated satellite galaxy against the mass ratio between the ESR and the total stars in the satellite. Results for both resolution runs are shown, with the solid line showing the median values. There is a strong correlation between M_* and the ESR mass fraction, with more less massive satellite galaxies containing a higher fraction of the ESR. In satellite galaxies with $M_* \sim 10^5 M_\odot$, the median mass fraction of the ESR is about 5 percent, in stark contrast to less than 0.004 percent in the satellite galaxies with $M_* \sim 10^9 M_\odot$ in the Auriga-L3.

Note that, the ESR fraction is unit in about 16 percent satellite galaxies in the Auriga-L3 galaxies. These systems have early star formation with an average star formation redshift of $z \approx 6.6$. After carefully examining the evolution of these systems, we find that they only experienced a single star formation event and subsequently ceased further star formation due to feedback and UV background heating. The stars in these satellite galaxies are thought to be enriched in alpha elements

($[\alpha/\text{Fe}] \sim 0.35$) and no significant scatter (e.g. Frebel & Bromm 2012). However, due to the lack of early metal production and mixing process in the Auriga simulation, we are unable to predict the detailed elemental abundance patterns of stars in these satellite galaxies.

It is noteworthy that some satellite galaxies, even those with masses greater than $10^8 M_\odot$, do not contain any ESR, as shown at the bottom of Fig. 6. About 16 percent of the satellite galaxies contain no ESR in the Auriga-L3 galaxies, indicating that their host dark matter halos have been polluted by surrounding galaxies before their first in-situ star formation episodes. These satellite galaxies have later star formation with an average star formation redshift of $z \approx 4.2$.

Although the quantitative ESR fraction values in these satellite galaxies depend on numerical resolution and the adopted sub-grid physics models, the qualitative results remain largely model independent, as shown in Fig. 6. Our results therefore suggest that the low mass and old satellite galaxies are best targets for searching for the ESR.

4. CONCLUSION

In this work, we have used the cosmological magnetohydrodynamic galaxy formation simulation Auriga to explore the total mass, spatial distribution, and kinematics of the ESR in Milky Way analogues. Our main findings are summarized as follows.

1. The formation time of ESR in the Auriga simulation spans a wide redshift range, from about $z = 22$ to $z = 4$. The averaged formation redshift of ESR is about $z = 10.0$, and the total mass fraction of ESR is tiny, about 2×10^{-5} of the entire stellar population in Auriga-L3.
2. The ESR tend to concentrate in the central region of the Auriga halos but are substantially less concentrated than the overall galactic stellar population. About half of the ESR reside within the 40 kpc of the galactic center.
3. Based on the orbital decomposition in the Auriga-L3, only a small fraction (about 4 percent) of ESR end up in the bulge component, about 8 percent ESR reside in the disk, and about 70 percent the ESR are distributed sparsely as halo stars, in particular the outer stellar halo, which contains more than 46 percent of the ESR.
4. The present day satellite galaxies contain significant fraction of ESR, accounting for about 18 percent of the total ESR in Auriga-L3. The ESR mass fraction of a satellite galaxy correlate strongly

with its stellar mass M_* , with lower mass satellite galaxies containing a higher fraction of ESR.

Our results suggest that the outer stellar halo and low mass faint satellite galaxies are the most promising sites to search for ESR. Since most of these stars are located in the outer regions of the Milky Way, the next generation of deeper survey projects, such as Chinese Space-station Survey Telescope (CSST), will help to greatly expand the ESR sample size. While some of the quantitative results may be influenced by numerical resolution, the qualitative results are largely resolution-independent. Therefore, the findings presented in this paper serve as a valuable guide for identifying the ESR in our Galaxy and, ultimately, contribute to constraining the properties of Pop III stars.

5. ACKNOWLEDGMENTS

HY are grateful to Shihong Liao for their useful discussions and comments. We acknowledge the supports from the National Natural Science Foundation of China (Grant No. 11988101) and the National Key Research and Development Program of China (Grant No. 2023YFB3002500). QG acknowledges the hospitality of the International Centre of Supernovae (ICESUN), Yunnan Key Laboratory at Yunnan Observatories Chinese Academy of Sciences, and European Union's HORIZON-MSCA-2021-SE-01 Research and Innovation programme under the Marie Skłodowska-Curie grant agreement number 101086388.

REFERENCES

- Abel, T., Bryan, G. L., & Norman, M. L. 2002, *Science*, 295, 93, doi: [10.1126/science.295.5552.93](https://doi.org/10.1126/science.295.5552.93)
- Aoki, W., Tominaga, N., Beers, T. C., Honda, S., & Lee, Y. S. 2014, *Science*, 345, 912, doi: [10.1126/science.1252633](https://doi.org/10.1126/science.1252633)
- Bromm, V., & Larson, R. B. 2004, *ARA&A*, 42, 79, doi: [10.1146/annurev.astro.42.053102.134034](https://doi.org/10.1146/annurev.astro.42.053102.134034)
- Bromm, V., & Yoshida, N. 2011, *ARA&A*, 49, 373, doi: [10.1146/annurev-astro-081710-102608](https://doi.org/10.1146/annurev-astro-081710-102608)
- Chen, L.-H., Pillepich, A., Glover, S. C. O., & Klessen, R. S. 2023, *MNRAS*, 519, 483, doi: [10.1093/mnras/stac3554](https://doi.org/10.1093/mnras/stac3554)
- Davis, M., Efstathiou, G., Frenk, C. S., & White, S. D. M. 1985, *ApJ*, 292, 371, doi: [10.1086/163168](https://doi.org/10.1086/163168)
- de Bennassuti, M., Salvadori, S., Schneider, R., Valiante, R., & Omukai, K. 2017, *MNRAS*, 465, 926, doi: [10.1093/mnras/stw2687](https://doi.org/10.1093/mnras/stw2687)
- El-Badry, K., Bland-Hawthorn, J., Wetzell, A., et al. 2018, *MNRAS*, 480, 652, doi: [10.1093/mnras/sty1864](https://doi.org/10.1093/mnras/sty1864)
- Frebel, A., & Bromm, V. 2012, *ApJ*, 759, 115, doi: [10.1088/0004-637X/759/2/115](https://doi.org/10.1088/0004-637X/759/2/115)
- Gao, L., Theuns, T., Frenk, C. S., et al. 2010, *MNRAS*, 403, 1283, doi: [10.1111/j.1365-2966.2009.16225.x](https://doi.org/10.1111/j.1365-2966.2009.16225.x)
- Gao, L., Yoshida, N., Abel, T., et al. 2007, *MNRAS*, 378, 449, doi: [10.1111/j.1365-2966.2007.11814.x](https://doi.org/10.1111/j.1365-2966.2007.11814.x)
- Grand, R. J. J., Gómez, F. A., Marinacci, F., et al. 2017, *MNRAS*, 467, 179, doi: [10.1093/mnras/stx071](https://doi.org/10.1093/mnras/stx071)
- Greif, T. H., Glover, S. C. O., Bromm, V., & Klessen, R. S. 2010, *ApJ*, 716, 510, doi: [10.1088/0004-637X/716/1/510](https://doi.org/10.1088/0004-637X/716/1/510)
- Greif, T. H., Springel, V., White, S. D. M., et al. 2011, *ApJ*, 737, 75, doi: [10.1088/0004-637X/737/2/75](https://doi.org/10.1088/0004-637X/737/2/75)
- Hartwig, T., Bromm, V., Klessen, R. S., & Glover, S. C. O. 2015, *MNRAS*, 447, 3892, doi: [10.1093/mnras/stu2740](https://doi.org/10.1093/mnras/stu2740)
- Heger, A., & Woosley, S. E. 2002, *ApJ*, 567, 532, doi: [10.1086/338487](https://doi.org/10.1086/338487)
- Hirano, S., & Bromm, V. 2017, *MNRAS*, 470, 898, doi: [10.1093/mnras/stx1220](https://doi.org/10.1093/mnras/stx1220)
- Ishigaki, M. N., Tominaga, N., Kobayashi, C., & Nomoto, K. 2018, *ApJ*, 857, 46, doi: [10.3847/1538-4357/aab3de](https://doi.org/10.3847/1538-4357/aab3de)
- Ishiyama, T., Sudo, K., Yokoi, S., et al. 2016, *ApJ*, 826, 9, doi: [10.3847/0004-637X/826/1/9](https://doi.org/10.3847/0004-637X/826/1/9)
- Jeon, M., Besla, G., & Bromm, V. 2017, *ApJ*, 848, 85, doi: [10.3847/1538-4357/aa8c80](https://doi.org/10.3847/1538-4357/aa8c80)
- Ji, A. P., Frebel, A., & Bromm, V. 2015, *MNRAS*, 454, 659, doi: [10.1093/mnras/stv2052](https://doi.org/10.1093/mnras/stv2052)
- Klessen, R. S., & Glover, S. C. O. 2023, *ARA&A*, 61, 65, doi: [10.1146/annurev-astro-071221-053453](https://doi.org/10.1146/annurev-astro-071221-053453)
- Li, H., Aoki, W., Matsuno, T., et al. 2022, *ApJ*, 931, 147, doi: [10.3847/1538-4357/ac6514](https://doi.org/10.3847/1538-4357/ac6514)
- Magg, M., Hartwig, T., Agarwal, B., et al. 2018, *MNRAS*, 473, 5308, doi: [10.1093/mnras/stx2729](https://doi.org/10.1093/mnras/stx2729)
- Magg, M., Schauer, A. T. P., Klessen, R. S., et al. 2022, *ApJ*, 929, 119, doi: [10.3847/1538-4357/ac5aac](https://doi.org/10.3847/1538-4357/ac5aac)
- Planck Collaboration, Ade, P. A. R., Aghanim, N., et al. 2014, *A&A*, 571, A16, doi: [10.1051/0004-6361/201321591](https://doi.org/10.1051/0004-6361/201321591)
- Reed, D. S., Bower, R., Frenk, C. S., et al. 2005, *MNRAS*, 363, 393, doi: [10.1111/j.1365-2966.2005.09416.x](https://doi.org/10.1111/j.1365-2966.2005.09416.x)
- Scannapieco, E., Kawata, D., Brook, C. B., et al. 2006, *ApJ*, 653, 285, doi: [10.1086/508487](https://doi.org/10.1086/508487)
- Schaerer, D. 2002, *A&A*, 382, 28, doi: [10.1051/0004-6361:20011619](https://doi.org/10.1051/0004-6361:20011619)

- Schaye, J., Crain, R. A., Bower, R. G., et al. 2015, MNRAS, 446, 521, doi: [10.1093/mnras/stu2058](https://doi.org/10.1093/mnras/stu2058)
- Sestito, F., Buck, T., Starckenburg, E., et al. 2021, MNRAS, 500, 3750, doi: [10.1093/mnras/staa3479](https://doi.org/10.1093/mnras/staa3479)
- Sotillo-Ramos, D., Bergemann, M., Friske, J. K. S., & Pillepich, A. 2023, MNRAS, 525, L105, doi: [10.1093/mnrasl/sl103](https://doi.org/10.1093/mnrasl/sl103)
- Springel, V. 2010, MNRAS, 401, 791, doi: [10.1111/j.1365-2966.2009.15715.x](https://doi.org/10.1111/j.1365-2966.2009.15715.x)
- Springel, V., White, S. D. M., Tormen, G., & Kauffmann, G. 2001, MNRAS, 328, 726, doi: [10.1046/j.1365-8711.2001.04912.x](https://doi.org/10.1046/j.1365-8711.2001.04912.x)
- Stacy, A., Bromm, V., & Lee, A. T. 2016, MNRAS, 462, 1307, doi: [10.1093/mnras/stw1728](https://doi.org/10.1093/mnras/stw1728)
- Starckenburg, E., Oman, K. A., Navarro, J. F., et al. 2017, MNRAS, 465, 2212, doi: [10.1093/mnras/stw2873](https://doi.org/10.1093/mnras/stw2873)
- Susa, H., Hasegawa, K., & Tominaga, N. 2014, ApJ, 792, 32, doi: [10.1088/0004-637X/792/1/32](https://doi.org/10.1088/0004-637X/792/1/32)
- Tegmark, M., Silk, J., Rees, M. J., et al. 1997, ApJ, 474, 1, doi: [10.1086/303434](https://doi.org/10.1086/303434)
- Wise, J. H., Turk, M. J., Norman, M. L., & Abel, T. 2012, ApJ, 745, 50, doi: [10.1088/0004-637X/745/1/50](https://doi.org/10.1088/0004-637X/745/1/50)
- Xing, Q.-F., Zhao, G., Liu, Z.-W., et al. 2023, Nature, 618, 712, doi: [10.1038/s41586-023-06028-1](https://doi.org/10.1038/s41586-023-06028-1)
- Yoshida, N., Abel, T., Hernquist, L., & Sugiyama, N. 2003, ApJ, 592, 645, doi: [10.1086/375810](https://doi.org/10.1086/375810)
- Yoshida, N., Omukai, K., Hernquist, L., & Abel, T. 2006, ApJ, 652, 6, doi: [10.1086/507978](https://doi.org/10.1086/507978)
- Zhu, L., Pillepich, A., van de Ven, G., et al. 2022, A&A, 660, A20, doi: [10.1051/0004-6361/202142496](https://doi.org/10.1051/0004-6361/202142496)